

**Pericyte actomyosin-mediated contraction at the cell-material interface can modulate the microvascular niche**

Sunyoung Lee<sup>1,\*</sup>, Adam Zeiger<sup>1,\*</sup>, John Maloney<sup>1</sup>, Maciej Kotecki<sup>2</sup>, Krystyn J. Van Vliet<sup>1,3,\*\*</sup>, and Ira M. Herman<sup>2,\*\*</sup>

<sup>1</sup>Department of Materials Science and Engineering, Massachusetts Institute of Technology,  
77 Massachusetts Avenue, Cambridge, Massachusetts 02139 USA

<sup>2</sup>Department of Physiology, Tufts University School of Medicine, 145 Harrison Avenue, Boston,  
Massachusetts 02111 USA

<sup>3</sup>Department of Biological Engineering, Massachusetts Institute of Technology,  
77 Massachusetts Avenue, Cambridge, Massachusetts 02139 USA

\*These authors contributed equally.

\*\*Co-corresponding authors: [krystyn@mit.edu](mailto:krystyn@mit.edu); [ira.herman@tufts.edu](mailto:ira.herman@tufts.edu)

*'This is an author-created, un-copyedited version of an article accepted for publication in Journal of Physics: Condensed Matter. IOP Publishing Ltd is not responsible for any errors or omissions in this version of the manuscript or any version derived from it. The definitive publisher authenticated version is available online at DOI:10.1088/0953-8984/10/000000*

**ABSTRACT:**

Pericytes physically surround the capillary endothelium, contacting and communicating with associated vascular endothelial cells via cell-cell and cell-matrix contacts. Pericyte-endothelial cell interactions thus have the potential to modulate growth and function of the microvasculature. Here we employ the experimental finding that pericytes can buckle a freestanding, underlying membrane via actin-mediated contraction. Pericytes were cultured on deformable silicone substrata, and pericyte-generated wrinkles were imaged via both optical and atomic force microscopy (AFM). The local stiffness of subcellular domains both near and far from these wrinkles was investigated by using AFM-enabled nanoindentation to quantify effective elastic moduli. Substratum buckling contraction was quantified by normalized change in length of initially flat regions of the substrata (corresponding to wrinkle contour lengths), and a model was used to relate local strain energies to pericyte contractile forces. The nature of pericyte-generated wrinkling and contractile protein-generated force transduction was further explored by the addition of pharmacological cytoskeletal inhibitors that affected contractile forces and the effective elastic moduli of pericyte domains. Actin-mediated forces are sufficient for pericytes to exert an average buckling contraction of 38% on the elastomeric substrata employed in these *in vitro* studies. Actomyosin-mediated contractile forces also act *in vivo* on the compliant environment of the microvasculature, including the basement membrane and other cells. Pericyte-generated substratum deformation can thus serve as a direct mechanical stimulus to adjacent vascular endothelial cells, and potentially alter the effective mechanical stiffness of nonlinear-elastic extracellular matrices, to modulate pericyte-endothelial cell interactions that directly influence both physiologic and pathologic angiogenesis.

## INTRODUCTION

Perivascular cells such as pericytes and vascular smooth muscle cells (SMCs) are mural cells that surround capillaries and post-capillary venules [3]. Pericytes are increasingly understood to play key roles in microvascular physiology and pathophysiology, including regulation of microvascular remodeling, maturation, and stabilization during angiogenesis (growth of new blood vessels) and lymphangiogenesis [6, 7]. Unlike SMCs, pericytes are actually embedded within the basement membrane, an extracellular matrix (ECM) comprising proteins such as fibronectin and collagen, which pericytes help to co-create in direct association with the capillary- and venular-derived endothelial cells. Both pericytes and SMCs of arterioles, veins and arteries establish intimate cell-cell contacts that serve to coordinate vascular tone and differentiation during development, adult life, and progression of vascular disease [6, 7]. Recently, it has been demonstrated that pericyte-endothelial cell interactions play a critical role in physiologic and pathologic angiogenesis [6, 11, 12]. These researchers focused primarily on the chemical interactions between endothelial cells and pericytes, including (i) the roles that basement membrane protein components play in modulating microvascular cell growth and contractile phenotype, or (ii) the regulatory roles that survival agents and growth factors play in signaling adaptive responses in cell-matrix associations via signaling pathways that modulate endothelial cell cycle kinetics and/or proliferative phenotype. Further, it has been shown that pericyte-endothelial interactions at gap junctions regulate microvascular dynamics during developmental or disease-associated phenomena [7].

Despite this recent and deepened understanding of the biochemical signal transduction regulating such varied phenomena as growth factor-receptor interactions, matrix adhesion, or electrochemical ion signaling via gap junctions [6, 7, 13, 14], little is known regarding the regulatory role of mechanical interactions between pericytes and endothelial cells. It is well established that other perivascular cell types such as SMCs [15-17] exert actomyosin-mediated contraction against extracellular matrices, and will actively counter externally applied tensile forces [18]. Such results strongly support the idea that pericytes and SMCs may play an important role in endothelial interactions, mechanotransduction, and angiogenesis. While biochemical signaling cascades and networks have been partially characterized as playing modulatory roles in regulating this pericyte function, mechanochemical or mechanical mechanisms by pericytes and SMCs have not yet been considered as important modulators of microvascular dynamics during physiologic or pathogenic processes.

Mechanical contact between pericytes and endothelial cells has been implied by an analysis of the intracellular cytoskeleton-dependent signaling pathways that are controlled by and reciprocally regulate the physical or chemical interconnections that exist among the actin network, plasma membrane and the associating extracellular matrix [7, 19, 20]. It is appreciated

that each cell is in communication with its microenvironment, transducing biochemical signals via basement membrane contacts, focal adhesion complexes, or cell-cell associations [21]. For example, activated transmembrane proteins termed integrins can bind to ECM ligands such as collagen or fibronectin, followed by intracellular signaling via membrane kinases, and cytoskeletal-associated effectors that tether the integrins to cytoskeletal actin filaments. Several Rho GTP-dependent signaling pathways [7] exert their influence on the actin-mediated mechanical force transduction by a multitude of effectors that include actomyosin- and actin-associated phosphoprotein kinases. Within the cell, mechanical forces are generated or destabilized through these downstream effectors, perhaps through actin filament polymerization, or via the inhibition of actomyosin-based contraction [22-24]. Importantly, integrins and associated adaptor proteins physically connect the intracellular actin stress fibers with the ECM and thereby provide a means to transmit actin-mediated forces to the extracellular environment. The role of integrins in mechanotransduction has been studied in SMCs [18, 25] and pericytes [19, 20]. For example, Kutcher et al. [7] used compliant silicone rubber substrata (poly(dimethyl siloxane), or PDMS) to show that wrinkling of the substrata resulted from the attachment forces transmitted from the actin cytoskeleton via integrins expressed on pericytes. However, these previous studies have focused primarily on the intracellular components and biochemical signaling aspects of pericyte adhesion, rather than force transduction by pericytes that may affect mechanical deformation or properties of adjacent basement membrane and vascular endothelial cells.

Here, we demonstrate that the actin filament assembly processes, including filament (de)polymerization and actomyosin-based contraction against a substratum material, play critical roles in regulating pericyte shape, contractility, cell-substratum attachment, force generation, and substratum deformation (i.e., general change in size or shape). As evidenced by wrinkle creation on PDMS substrata [7], the dynamic deformation of ECM ligand-coated substrata implies that mechanotransduction mediates pericyte adhesion to and deformation of underlying substrata. Our atomic force microscopy (AFM)-based imaging of the living pericytes' deformation of compliant substrata demonstrates the regulatory role of actin filaments and actomyosin contractions in generation of mechanical forces required for cells to sustain their shape and sustain contractile phenotype. Further, by using pharmacological cytoskeletal inhibitors (latrunculin A, blebbistatin, ML-7, nocodazole, and jasplakinolide), we dissect the relative contributory roles of actin dynamics and actin-myosin interactions in regulating pericyte-generated deformation of PDMS substrata, including the local cell stiffness as measured by AFM-enabled indentation. These results indicate that the actin cytoskeleton is a critical cellular integrator required to sustain pericyte morphology and membrane tension. Further, AFM imaging of the wrinkled substrata enables our quantification of cell-induced

substrata deformation, which in turn allows us to estimate the forces and stresses that can be exerted by pericytes. We ascertain that these mechanical forces could be sufficient to not only directly deform nearby cells, but could also modify in turn the local effective elastic properties of the adjacent extracellular matrix. Either mechanism – direct pericyte-generated mechanical stimulus to adjacent vascular endothelial cells or modification of the effective mechanical stiffness of nonlinear-elastic extracellular matrices – can thus serve to modulate pericyte-endothelial cell interactions that directly influence both physiologic and pathologic angiogenesis of the microvascular niche. These findings point to an important new role for mechanical force transduction in regulating cell-matrix and microvascular cell-cell dynamics during physiologic or pathologic angiogenesis.

## **MATERIALS AND METHODS**

### **Cell culture**

Pericytes were cultured from capillary fragments isolated from mammalian (bovine) retinas as previously described [26]. Briefly, capillary fragments were isolated by collagenase digestion of minced retinas followed by sieving. The capillary fragments were plated into tissue culture flasks in Dulbecco's modified Eagle's medium (DMEM) supplemented with 10% calf serum. The pericytes were identified and distinguished from endothelial cells by their larger size and irregular morphology, by their noncontact-inhibited growth patterns, by their staining with anti-3G5 IgG, anti-smooth muscle actin IgG and the lack of staining with di-I-acyl-LDL and antisera to bovine Factor VIII. These criteria were established by Herman and D'Amore [26] and subsequently used by others to identify capillary pericytes.

### **Synthesis and functionalization of deformable silicone substrata**

Use of silicone as deformable substrata for at least qualitative observation of contractile cells was initially demonstrated by Harris et al. and others, and quantified by Burton et al. [27-29]; this system has also been employed in previous pericyte studies [26]. Deformable silicone films, supported by liquid silicone, were prepared as described previously [7, 27]. Briefly, 6  $\mu$ L of poly(dimethyl siloxane) (PDMS, Sigma-Aldrich) was pipetted using a positive displacement pipettor onto round glass coverslips of 12 mm diameter. The PDMS was permitted to spread at room temperature prior to thermal cross-linking, achieved by passing the PDMS-coated coverslip through a Bunsen burner flame. The PDMS-coated coverslip was then placed within a glow discharge apparatus [7, 30], which is comprised of an anode, a cathode for generating a glow discharge between the cathode and the anode upon application of a negative pulse, and a triggering electrode for starting the glow discharge. This approach has been successful in creation of hydrophilic surfaces, e.g., Formvar-coated electron microscope grids coated with

carbon, as the glow discharge apparatus places an electrically discharged plasma onto the surface of the silicone; this enhances hydrophilicity of PDMS and permits coating with extracellular matrix proteins, (here, 100  $\mu$ L of 0.1 mg/mL rat tail collagen Type-I (BD Biosciences, cat. #354236) in Tris-HCl buffer at pH 7.4) and the subsequent attachment of pericytes.

### **Measurement of local elastic moduli and AFM contact mode imaging**

An atomic force microscope (AFM; PicoPlus, Agilent Technology) was incorporated within an inverted optical microscope (IX81, Olympus) to enable facile positioning of AFM cantilevered probes above pericyte apical surfaces (See Figs. 1 – 3). All imaging and mechanical characterization experiments were conducted on living pericytes in full media at room temperature. Calibration of AFM cantilevers of nominal spring constant  $k = 0.01$  nN/nm and probe radius  $R = 25$  nm (MLCT-AUHW, Veeco) was conducted as described previously [31-33]. Briefly, inverse optical lever sensitivity [nm/V] (InvOLS) was measured from deflection-displacement curves recorded on rigid glass substrates. Spring constants [nN/nm] of AFM cantilevers were measured via thermal activation recording of deflection, and the Fast Fourier Transform of cantilever free-end amplitude as a function of oscillation frequency was fitted as a harmonic oscillator to obtain  $k$ . For each measurement of effective elastic moduli at any given location on any given cell, at least 30 replicate indentations were acquired to maximum depths of 10 nm. At least five cells were analyzed for each condition, and multiple wrinkles (i.e., indentation locations) were associated with each cell, as indicated in figure captions. Acquired probe deflection-displacement responses were converted offline (Scanning Probe Imaging Processor, Image Metrology), using measured spring constants and InvOLS, to force-depth responses. Effective elastic moduli  $E$  were calculated by applying a modified Hertzian model of spherical contact to the loading segment of the force-depth response, as detailed elsewhere [33, 34] with the scientific computing software Igor Pro (Wavemetrics). These values represent the local stiffnesses of the subcellular domains (hereafter, termed microdomains) probed in each experiment under contact loading, and are not intended to indicate the elastic properties of the entire cell or the Young's elastic modulus under uniaxial loading. The actual volumes of cells probed in each indentation can only be estimated at present; from the contact widths of 40 nm and depths of 10 nm, a reasonable estimate for an elastically strained region of the cell would be a sphere of 25 nm radius comprising a volume on the order of 65,000 nm<sup>3</sup>. Computed elastic moduli  $E$  are reported as average +/- standard deviation, and all statistical analyses were conducted with one-way ANOVA (Tukey analysis).

Before AFM contact mode imaging and elastic moduli measurement,  $x$ - and  $y$ -axes hystereses in the closed loop scanner were calibrated to improve the positioning of AFM

cantilevered probes on pericyte membranes and PDMS substrata. The force that AFM cantilevers exerted on pericyte membranes during contact mode imaging did not exceed 500 pN, which was chosen to minimize distortion of features such as cortical actin in the living cells. Pericytes that changed morphology or attachment on PDMS substrata due to the AFM imaging and mechanical tests were excluded from further analysis.

### **Determination of contraction exerted by pericytes on PDMS**

When the living, contractile pericytes were imaged via AFM, the topography of the wrinkled PDMS substrata was also mapped simultaneously. Such topographical information provided by AFM height images (Fig. 4) allows pericyte-exerted contraction to be quantified. This cell contraction induced the buckling that resulted in the observed wrinkles on the PDMS substratum. Cell-exerted contraction was inferred from analysis of the wrinkle topography in AFM height images. This contraction is defined and quantified herein as the normalized change in length of the initially unwrinkled substratum region:  $c = (\text{final length} - \text{original length of PDMS span}) / \text{original length} = (l_f - l_o) / l_o$ . Here, it is implicitly assumed that the cell was in contact (via focal adhesive complexes) with the substratum on both sides of a wrinkled span. Wrinkle lengthspan  $l_f$  and initially unwrinkled lengthspan  $l_o$  are calculated from the wrinkle wavelength and contour length, respectively, of the wrinkles in topography or height images of the wrinkled PDMS obtained in AFM contact mode. (Note that this buckling contraction, though consisting of a normalized length expressed as a percentage, does not correspond to the material strain experienced by the PDMS itself. Instead, it represents the change in length between two points at the cell-material interface, due to wrinkling induced by cell contraction.) This analysis makes the reasonable assumption that the PDMS region ( $l_o$ ) was flat prior to cell contraction. The original length was determined from the arc length of the wrinkle by approximating the wrinkle as a sinusoidal curve of amplitude  $A$  and wavelength  $\lambda$ . The arc length is equal to

$$l_o = \int_0^\lambda \left[ \left( \frac{dy}{dx} \right)^2 + 1 \right]^{1/2} dx \quad (1)$$

where

$$y(x) = A \cdot \sin(2\pi x / \lambda). \quad (2)$$

More than thirty images, comprising a total of 71 wrinkles ( $n = 71$ ), were analyzed for this strain calculation, and data are reported as average +/- standard deviation.

### Estimation of pericyte-exerted force and stress

Other groups have modeled the coupling between contractile force and wrinkle amplitude and wavelength in freestanding membranes [35] and thin films on substrates [36]. Determining the applied force required to induce wrinkling of thin films and membranes is a complex problem governed by non-linear, partial differential equations [35]. These equations remain unsolved, except by semi-analytical methods in specific one-dimensional cases, which do not include the present circumstance of wrinkling induced by compression of an isolated region within a membrane.

It is possible to estimate pericyte-exerted force by totaling the strain energy accumulated in the substrata upon contraction to a given level of  $c$ , and equate this to the work done by the cells via contraction. We idealize the pericytes' contraction mechanism (i.e., the array of focal adhesions) as a force-exerting strip, (Supplemental Figure 1), and subdivide the film into multiple equivalent regions that encompass the distance from the cell center to the midpoint between this cell and the nearest neighboring cell. We take the region width to equal the width of the wrinkled area  $W$ , as shown in Supplemental Figure 1. We note that each region can be divided into a wrinkled area ( $d_1 \times W$ ) of wrinkle wavelength  $\lambda$  that undergoes compressive stress (corresponding to the bending strain energy over distance  $d_1$ ) and an area beyond the cell ( $d_2 \times W$ ) that undergoes tensile stress (corresponding to the stretching strain energy over distance  $d_2$ ). The total exerted energy of this deformation is the sum of these bending and stretching components. The bending strain energy of the compressed area is

$$U_B = Wd_1D(d^2y/dx^2)^2/2 \cong Wd_1D\lambda^2/2 \quad (3)$$

where  $D$  is the flexural rigidity of the film  $Et^3/[12(1-\nu^2)]$  and  $E$  is the Young's elastic modulus of the PDMS [37]. The normal (stretching) strain energy of the area under tension is

$$U_N = Wd_2t(\delta/d_2)^2E/2 = Wt\delta^2E/2d_2 \quad (4)$$

where  $\delta$  is half the difference between the unwrinkled contour length  $l_0$  and the final point-to-point distance  $l_f$ , and thus represents the distance over which the cell exerted contractile force. As discussed in Results, we found that the stretching energy  $U_N$  was the larger or dominant term for the case of pericytes wrinkling such PDMS substrata. Moreover, this is a minimum estimate of the stretching energy, since the region of PDMS stretched to nonzero displacements likely extends beyond the region defined by



the rectangular strip of dimensions  $d_2 \times W$ . We thus set  $U_N$  equal to the work done by the contractile machinery on one side of the cell, or

$$U_N \approx F\delta/2 \quad (5)$$

We then obtain the local, cell-generated force  $F$  corresponding to this wrinkling:

$$F \approx EWt\delta/d_2 \quad (6)$$

### **Measurement of PDMS uniaxial stress-strain response and elastic moduli**

To determine the Young's elastic modulus of the PDMS substrata  $E_{\text{PDMS}}$  and to ascertain whether this material exhibited a nonlinear elastic response over the range of pericyte-exerted strains, uniaxial tension experiments were conducted on freshly prepared PDMS films. PDMS was prepared according to the thermal crosslinking protocol of Harris et al., as recommended for preparation of thicker layers than achievable via flaming [27]. However, we lowered the oven temperature to 275°C to avoid vaporization and redeposition of unreacted siloxanes during thermal curing. Here, 50 mL of polydimethylsiloxane (Sigma-Aldrich DMPS12M; viscosity of 12.25 Pa·s at 25°C) was poured into a glass petri dish of 100 mm diameter. Before pouring, Teflon™-coated paper was added to the bottom of the petri dish to prevent adhesion of PDMS to the glass, and placed in an oven for 3 h at 275°C. After allowing the sample to cool to room temperature in the vented oven, rectangular samples (approximately 6 cm long x 1.5 cm wide x 0.65 cm thick) were cut and carefully removed from the dish. Uniaxial tensile grip regions were fashioned by mounting the sample ends between two thick cardboard squares secured with five-minute-curing epoxy (Loctite, Henkel). Uniaxial tension experiments (8848 Microtester, Instron) were conducted in displacement control at 75 μm/s to the point of fracture failure within the gage section. Young's elastic modulus  $E_{\text{PDMS}}$  ( $2.1 \pm 0.3$  MPa,  $n = 2$ ) was calculated via a best-fit linear regression to the entirety of the loading response; at these displacement rates, the engineering stress-engineering strain response was approximately linear up to the maximum engineering fracture strain of 27%.

### **Fluorescence microscopy imaging – F-actin staining**

Pericytes were fixed with 4% paraformaldehyde for 15 min at room temperature, followed by membrane permeation with 0.1% Triton-X solution in 150mM NaCl phosphate buffered saline (PBS) for 3 min. Pericytes were then incubated with Alexa Fluor 488 phalloidin (green, Invitrogen, 1:300 dilution from stock) for 1 hr at room temperature. Pericytes were rinsed three times (5 min each) with PBS and then imaged by fluorescence microscopy (IX81, Olympus).

## RESULTS

Effective elastic moduli (or stiffness) of pericyte subcellular domains were measured through AFM-enabled nanoindentation (see Materials and Methods). Pericytes were grown on collagen-conjugated PDMS (Fig. 1A), and AFM probes of radius  $R = 25$  nm were placed at specific positions, such as pericyte plasma membranes positioned over regions of substrata deformation sufficient to generate visible wrinkles in the PDMS. In contrast, AFM probes were also positioned above pericyte domains that were far from wrinkles in the PDMS substrata (Fig. 1). To increase the efficiency of the positioning of AFM probes on specific regions of the cells, live pericytes were first imaged in AFM contact mode. Using a closed loop piezoscanner, the positions of AFM probes on pericyte membranes were chosen to enable the measurement of local elastic moduli at positions both “on” and “off” the wrinkles that were generated ostensibly by the pericyte contraction of the PDMS substrata (Figs. 1 – 3). Here, the terms “on” and “off” describe positions on the pericyte apical surface that are above wrinkled and nonwrinkled regions of the PDMS substrata, respectively. See Materials and Methods for detailed information about AFM imaging and measurement. Figure 1B and C illustrate the integrated optical microscopy and AFM imaging of pericytes. We hypothesized that the pericytes generated wrinkles on the PDMS substrata via actin-mediated force exertion due to mechanisms such as actin polymerization and actomyosin contraction. Thus, we reasoned that the pericytes

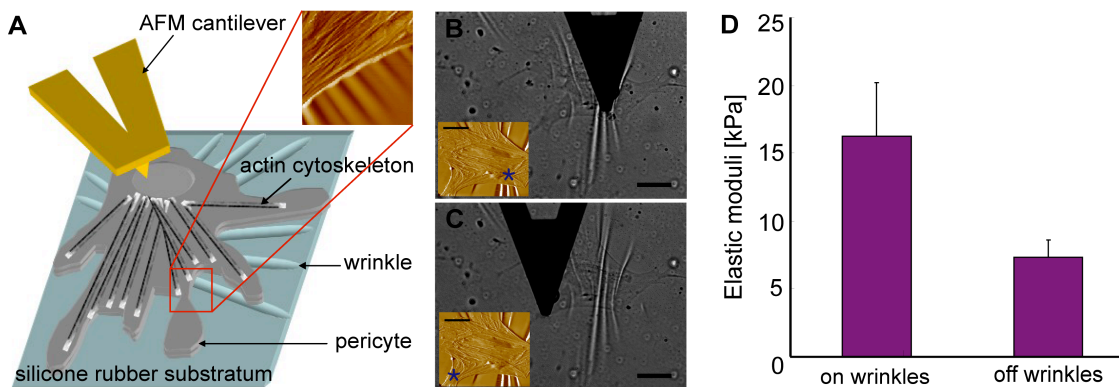


FIGURE 1 (A) Schematic of AFM-enabled imaging and indentation. Cell and wrinkle topography was obtained from contact-mode imaging. Effective elastic moduli were determined via indentation at specific subcellular regions of interest on the pericyte, using optical microscopy to position the probe both “on” or above substrata wrinkles (B) and “off” or far from wrinkles (C). Inset images in (A)-(C) are AFM deflection images, and blue asterisks (\*) indicate corresponding locations of indentation. (D) summarizes effective elastic moduli of pericyte microdomains both on ( $16.3 \pm 3.9$  kPa) and off ( $7.4 \pm 1.1$  kPa) these wrinkles (see Methods). Error bars denote standard deviation. Scale bars = 20  $\mu$ m.

would exhibit greater stiffness near the wrinkles, likely due to the force transduction transferred from bundled actin arrays that are crosslinked to membrane domains anchored in the extracellular matrix via integrin-focal adhesion protein assemblies. The effective elastic moduli  $E$  of the pericyte subcellular domains measured directly above or “on” wrinkles, near the apparent origin of these wrinkles, and far from or “off” these wrinkles were measured through optical microscopy-aided AFM as schematized in Fig. 1. As indentation depths were restricted to  $< 25$  nm to allow more spatially resolved analysis, here  $E$  is representative of the microdomain stiffness of the cell’s cortical actin and cytoplasm (rather than of the whole cell). AFM-enabled nanoindentation (Figs. 1A, 2, and 3) showed that the effective (average) elastic moduli at off-wrinkle locations of the pericytes were 45.4% less than that at on-wrinkle

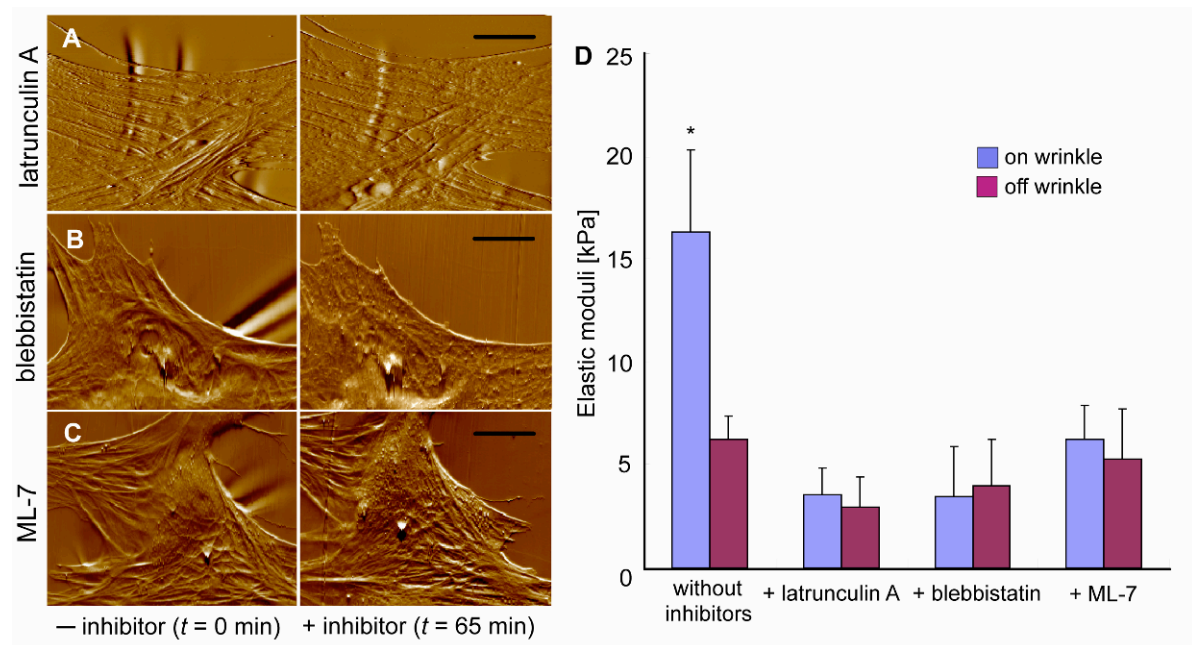


FIGURE 2 Actin-dependent alterations in pericyte shape, contractile phenotype and elastic moduli of cell microdomains. In (A), (B), and (C), AFM deflection images demonstrate changes in pericyte shape. Concomitantly, cell shape and PDMS deformation, either before or 65 min after the addition of pharmacological inhibitors that specifically affect actin (de)polymerization and/or actomyosin contraction: (A), latrunculin A (1  $\mu$ M); (B), blebbistatin (25  $\mu$ M); (C), ML-7 (300 nM), respectively (see Table 1). (D) demonstrates the elastic moduli of pericyte microdomains (see Materials and Methods), before and after addition of inhibitors, both on and off deformed (wrinkled) regions. Table 2 summarizes elastic moduli with inhibitors. For each condition,  $n > 5$  cells were considered, and 30 indentations were acquired at each point (on/off wrinkle positions). Error bars denote standard deviation. Scale bars = 20  $\mu$ m. Asterisk (\*) indicates statistically significant difference from all other conditions and positions (on/off wrinkle) shown ( $p < 0.01$ ).

TABLE 1 Pharmacological cytoskeletal inhibitors and concentrations used in this study.

| Chemical                  | Binding target            | Mechanisms and consequences  |
|---------------------------|---------------------------|--|
| Latrunculin A (1 $\mu$ M) | Monomeric G-actin         | Binds to actin monomers, making 1:1 complexes with monomers. This thus inhibits actin polymerization and disruption of the actin cytoskeleton [1].   |
| Blebbistatin (25 $\mu$ M) | Myosin ATPase             | Binds to myosin ATPase and thus blocks force exertion by actomyosin contraction. Cellular consequence is that microtubules dominate over the actin cytoskeleton in maintenance of cell morphology and force generation in contrast to the effects from nocodazole [2].   |
| ML-7 (300 nM)             | Myosin light chain kinase | Binds to myosin light chain kinase, thus blocks the force generation of actomyosin contraction, inhibiting myosin light chain phosphorylation. Therefore, ML-7 acts as a competitive inhibitor against ATP for actomyosin contraction [4, 5].  |
| Nocodazole (660 nM)       | $\beta$ -tubulin          | Binds to $\beta$ -tubulin and thus blocks microtubule assembly, disrupting microtubule dynamics during interphase and inhibits spindle formation during mitosis. Cellular consequences include inhibition of karyokinesis during M-phase while altering the actin-dependent contribution to cell morphology and force generation during interphase by disrupting cellular balance between actin and microtubule networks [2, 8]. |
| Jasplakinolide (660 nM)   | Actin filament (F-actin)  | Binds to actin filaments, inducing large F-actin aggregates. Cellular consequences include the enhancement of the rate of actin polymerization, stabilizing actin filaments <i>in vitro</i> [9, 10].   |

TABLE 2 Elastic moduli of pericyte microdomains with pharmacological inhibitors.

| Elastic modulus [kPa] | Media only (control) | Latrunculin A | Blebbistatin  | ML-7          | Nocodazole     | Jasplakinolide |
|-----------------------|----------------------|---------------|---------------|---------------|----------------|----------------|
| On wrinkles           | 16.3 $\pm$ 3.9       | 3.5 $\pm$ 1.3 | 3.5 $\pm$ 2.4 | 6.3 $\pm$ 1.6 | 16.8 $\pm$ 6.9 | 18.1 $\pm$ 6.4 |
| Off wrinkles          | 6.3 $\pm$ 1.1        | 2.9 $\pm$ 1.5 | 4.0 $\pm$ 2.2 | 5.3 $\pm$ 2.4 | 7.2 $\pm$ 2.8  | 7.4 $\pm$ 3.1  |

positions ( $n = 150$ , Fig. 1D and Table 2). Here, pericytes that changed the number of wrinkles, attachment to substrata, or cell morphology during the course of such mechanical tests were excluded from analyses. To consider the possibility that this increased  $E$  of the cell on locations of PDMS wrinkles could be due to an increase in the effective mechanical stiffness of wrinkled PDMS itself, elastic moduli of wrinkled and unwrinkled PDMS were measured at locations just outside the cell perimeter;  $E_{\text{PDMS}}$  on and off such wrinkles were not statistically significantly different ( $n = 4$  wrinkles,  $p > 0.05$ ).

We hypothesized that PDMS substrata deformation by pericytes and the change in the elastic moduli of local pericyte membrane microdomains were attributable to the organization and contraction of the actin cytoskeleton. Internally generated mechanical forces could then be transduced across the cell surface to the underlying substrata via filament assembly/disassembly, membrane-associated crosslinking, and, possibly, actomyosin-based contraction. As reported by Shlomovitz et al. [38], these actin-based forces are closely coupled. As has been reported,

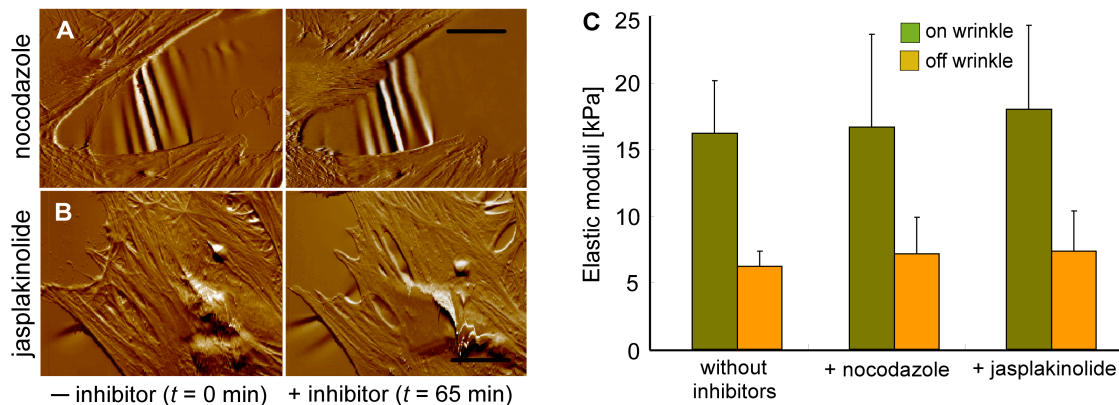


FIGURE 3 Change in elastic moduli and cell shape with addition of cytoskeleton-modulating agents. The same set of experiments as shown in Fig. 2 was conducted with pharmacological reagents that increase the activity of the actin cytoskeleton: nocodazole (670 nM) (A) and jasplakinolide (670 nM) (B): see Table 1. (C) Mechanical tests were conducted before and after addition of these reagents at cell membranes on and off PDMS wrinkles. See Table 2 for summary of elastic moduli with nocodazole and jasplakinolide. All the mechanical tests were conducted with more than five cells ( $N = 5$ ) and 30 mechanical tests ( $n = 30$ ) on and off wrinkles. **Error bars denote standard deviation.** Scale bars = 20  $\mu\text{m}$ .

integrin receptors can physically link ECM ligands and the actin cytoskeleton, generating mechanical forces that are apparently sufficient to deform PDMS substrata to create wrinkles [7]. To verify this hypothesis, we measured the stiffness of pericyte microdomains before and after the addition of direct actin- and actomyosin-inhibiting pharmacological agents (latrunculin A, blebbistatin, and ML-7), as well as additional agents that only peripherally modulate actin polymerization and actomyosin-based contraction (nocodazole and jasplakinolide [1, 2, 4, 5]; see Table 1 for mechanisms of action and working concentrations). We have considered the steady-state or maximal inhibition state at room temperature, which would also be achieved *in vivo* at 37°C but at a rate corresponding to that elevated temperature. Reduced substrata deformation is indicated by the decreased number of wrinkles that pericytes generate due to the inhibition effect of these reagents, as shown in Fig. 2. In the absence of actin-specific reagents, however, the number of wrinkles did not decrease over time. This confirms that the force exerted by pericytes on the underlying substrata decreased in the presence of reagents that acted on the actin network (latrunculin A) and actomyosin contractile processes (blebbistatin and ML-7). Correspondingly, the effective elastic moduli  $E$  of the pericyte microdomains decreased both on and off wrinkles due to the pharmacological inhibitors (see Table 2 for summary of elastic moduli +/- inhibitors). This decrease in the local stiffness of pericytes was caused by the reduced density (by 25%) and approximate diameter (by 13%) of actin stress fibers, as quantified by AFM contact-mode height images of these cells. At 65 minutes after the addition of latrunculin A, blebbistatin, and ML-7 at room temperature,  $E$  on-wrinkles and off-wrinkles

was not statistically different, which indicates the dominant effect of the actin cytoskeleton on the local stiffness of the pericyte surface microdomains. Optical microscopy images of phalloidin-stained F-actin within the pericytes (Supplementary Fig. 2) after the addition of latrunculin A, blebbistatin, and ML-7 reveal cytoskeletal reorganization as the cell cortex blebs and peripheral membrane domains are observed to bulge into irregular, rounded membrane structures. Comparison among these different pharmacologically inhibited populations shows that the actin stress fibers still remained visible 1 hour after treatment with ML-7 and latrunculin A, while pericyte morphology and the number of actin stress fibers changed dramatically with blebbistatin. Both the morphological and microstructural changes indicate the loss and/or decrease of actin-mediated intracellular forces under these challenges.

When inhibitors were washed out via replacement with fresh media, pericytes recovered these substrata wrinkles within 45 min at 37°C (data not shown). Pericytes that were not treated with pharmacological inhibitors did not lose the capacity to maintain wrinkles in the substrata. Correspondingly, pericyte microdomain stiffness did not change over this same imaging duration, and cells exhibited distinct actin stress fibers in epifluorescence images of actin-stained pericytes (Supplementary Figure 2).

Nocodazole and jasplakinolide were next considered as indirect, positive modulators of actomyosin contraction. Nocodazole, which binds to microtubule monomers ( $\beta$ -tubulin) and inhibits the microtubule polymerization, is a pharmacological inhibitor that indirectly activates the actin cytoskeleton while jasplakinolide can induce polymerization of the actin cytoskeleton

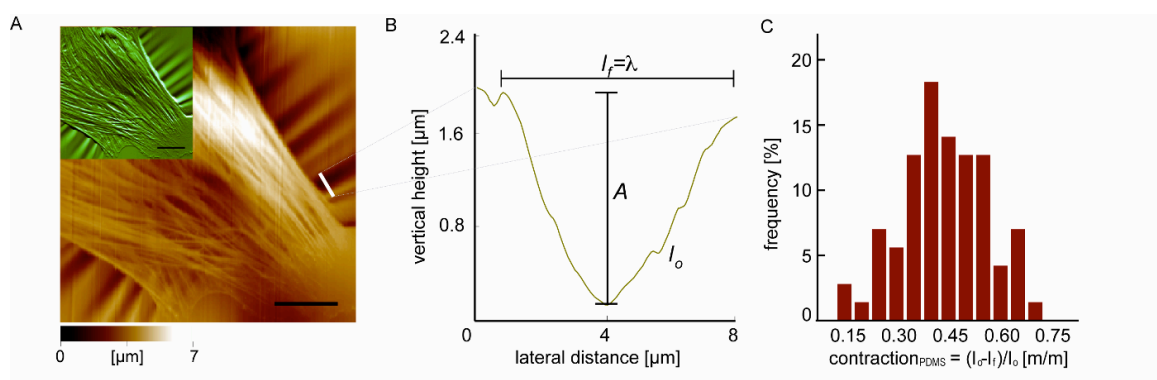


**FIGURE 4** Calculation of contraction induced by pericytes. (A) AFM contact-mode topography image indicates height changes of wrinkled PDMS substrata; inset: corresponding deflection (error-signal) image for same pericyte. Scale bar = 20  $\mu\text{m}$ . From wrinkle topography, pericyte-exerted force on the PDMS substrata can be estimated as described in the text. (B) Height trace of one such wrinkle, indicated as white line in (A). Contraction of the PDMS, defined as the normalized change in length between two points due to wrinkling  $(l_0 - l_f) / l_0$ , of  $37.5 \pm 1.8\%$  was calculated from the final wrinkle span  $l_f$  and initial unwrinkled length  $l_0$  (see Materials and Methods);  $n = 71$  wrinkles. (C) Distribution of contraction observed.

(see Table 1). We hypothesized that both nocodazole and jasplakinolide might enhance the ability of pericytes to generate mechanical forces sufficient for substratum deformation and alter local elastic moduli. This hypothesis was due in part to our results from latrunculin A, blebbistatin, and ML-7, which demonstrated the critical contribution of the actin cytoskeleton in the creation of wrinkles on substrata. Pericytes were imaged in AFM contact mode, followed by indentation of pericyte microdomains on- and off-wrinkles to obtain  $E$ , before and 65 min after the addition of these inhibitors. Microdomain stiffness at locations of cell-induced wrinkling either increased or remained unchanged in response to nocodazole and jasplakinolide. (See Table 2 for summary of elastic moduli with inhibitors.) Fluorescent images with actin-stained pericytes after incubation with nocodazole demonstrated that the thickness of actin stress fibers increased with decreasing spacing between actin stress fibers (Supplementary Fig. 2), whereas jasplakinolide-treated pericytes showed brighter, thickened actin-concentrated patches on stress fibers. Statistically similar or increased  $E$  with nocodazole and jasplakinolide (Fig. 3C and Table 1) were consistent with the finding that the number of pericyte-generating wrinkles increased or did not change under optical fluorescence microscopy and AFM contact-mode imaging. Together, these results show that the mechanism under which pericytes generate wrinkles on the PDMS substrata was directly related to the force-generating potential of actin cytoskeletal dynamics.

In order to calculate the forces required to generate wrinkles on the PDMS substrata, one may first consider approaches similar to Cerda et al. [35]. However, alternate wrinkling analyses such as Cerda et al. [35] and Chung et al. [36] consider a tensile loading of an entire film that does not appear analogous to local, orthogonal compression beyond the critical point. Those models thus would predict unphysical compressive strains exceeding 100% and thus are not adopted for our analysis of cell-induced contraction. Above the critical strain required for buckling, deformation of a freestanding membrane or film-on-substrate becomes a complex analytical problem beyond the scope of this paper. Instead, we adopted the model outlined in Materials and Methods. From our analysis of the wrinkle contours, we computed the strain exerted by pericytes that was required to induce the observed percent contraction and degree of PDMS wrinkling. This was an analysis of contraction of the pericytes (the “cell side” of this cell-material interface) based upon observations of wrinkling of the substratum (the “material side” of this interface). From Eqs. 1 and 2, we found that pericytes thus exert a contraction of  $37.5 \pm 1.8\%$  (average  $\pm$  standard error of measurement), ranging from 6 to 67%, to wrinkle this substratum under basal culture conditions.

To estimate the cell-generated traction force and stress corresponding to this wrinkling, we related the strain energy of substratum deformation to the work done by the pericyte. As outlined in Materials and Methods, such calculation of strain energies requires experimental

input parameters related to the contractile displacement  $\delta$  ( $0.6 \pm 0.05 \mu\text{m}$ ) and wrinkle wavelength  $\lambda$  ( $7.6 \pm 0.2 \mu\text{m}$ ) quantified via AFM topography; Young's elastic modulus  $E$  ( $2.1 \pm 0.3 \text{ MPa}$ ), thickness ( $t = 1 \mu\text{m}$  [39]), and Poisson's ratio ( $\nu = 0.5$ ) of this PDMS substratum; and typical wrinkle widths  $W$  ( $100 \mu\text{m}$ ), length span comprising the wrinkled regions  $d_1$  ( $20 \mu\text{m}$ ), and midpoint distance  $d_2$  ( $100 \mu\text{m}$ ) taken from optical microscopy images such as Figs. 1B, C. For these data, the minimum estimate for the stretching energy  $U_N$  exceeds the bending energy  $U_B$  (Eqs. 3-4). Equation 5 then indicates the cell-generated force  $F = 1.4 \pm 0.1 \mu\text{N}$ , which is in reasonable agreement within an order of magnitude to that reported by others for other cell types on similar PDMS substrata (i.e., the force applied tangential to the substratum that is required to induce wrinkle profiles comparable to those induced by cell contraction on these substrata, as measured by calibrated microneedles) [29, 40].

It is possible to continue the model to estimate the tractional stress exerted at the focal adhesions by pericytes by estimating the quantity, location, and size of the individual adhesion sites. For example, if we model the region of force application (defined by the periphery of the cell comprised of fifty focal adhesions each of radius  $1 \mu\text{m}$ ), then the traction exerted by the cell is approximately  $8.8 \pm 0.6 \text{ kPa}$  per focal adhesion complex. This traction represents an order of magnitude approximation of pericyte-exerted stress per focal adhesion, and is similar to traction reported for other cell types by other measurement methods [41-43].

Thus, this model provides a useful and reasonable order of magnitude estimate of cell-exerted force with a simple analysis that does not require the use of calibrated microneedles or micropatterned substrates. We therefore conclude that an AFM map of topography enables cell-generated force to be estimated by the elasticity analysis proposed. This is also the first demonstration of the use of wrinkling topography to directly relate the magnitude of forces exerted specifically by pericytes on adjacent substrata, and further elucidates the capacity of specific cytoskeletal inhibitors and agonists to mediate this traction.

## DISCUSSION AND CONCLUSIONS

Microvascular pericytes are mural cells that modulate capillary tonus and endothelial growth potential, events that are critical to physiologic and pathological angiogenic phenomena during human development and vascular disease states. Here, AFM-based mechanical testing enabled the quantification of force transduction by microvascular pericytes, including effective stiffness of cell microdomains near and far from regions of cell-generated substratum wrinkling. Quantitative analysis of the origins of pericyte-generated force transduction and substrata deformation was enabled by the addition of cytoskeletal-specific pharmacological disrupting agents/inhibitors. F-actin-mediated substratum deformation was observable via changes in cell shape and local stiffness, which corresponded to F-actin assembly and/or actomyosin-dependent



ATPase-mediated contraction. These substrata deformations enable estimates of cell-induced contraction, both to facilitate comparison with other contractile cell types and to consider the potential changes in elastic properties of biological ECM that are considerably more complex than the present PDMS substrata.

Pericytes are capable of generating sufficient force to underlying PDMS substrata, inducing wrinkles on collagen-coated PDMS substrata as shown in Fig. 1. We hypothesized that these wrinkles were generated by mechanical forces via the actin cytoskeleton and actomyosin-based contraction. To verify this hypothesis, we determined effective elastic moduli of pericyte membranes “on” (i.e., above) substrata wrinkles and “off” (i.e., far from) wrinkled regions. As summarized in Table 2, effective elastic moduli of pericyte microdomains off-wrinkles were 45% lower than those on-wrinkles, which implied that the creation of wrinkles on PDMS substrata was mediated by stiff actin bundles and actin-related force exertion such as filament assembly and actomyosin contraction. The pharmacological inhibitors, including latrunculin A, blebbistatin, and ML-7, triggered the loss of wrinkles as visualized through optical microscopy and AFM contact mode imaging. Mechanical measurements of pericyte microdomains showed a decrease in local elastic moduli after the addition of these inhibitors, implying that the actin cytoskeleton maintains mechanical stiffness near the apical cell surface. These results were supported by fluorescence optical microscopy images that showed the resulting changes in cell morphology and the density of the F-actin cytoskeleton. In contrast, nocodazole and jasplakinolide, which indirectly and directly activate the actin cytoskeleton, respectively, increased or retained the microdomain stiffness. This result was consistent with AFM and optical images showing that the number of wrinkles created on PDMS substrata were also maintained or increased for these pharmacological challenges. By employing these nanomechanical tests, optical / fluorescence microscopy and AFM imaging approaches, we demonstrated that the actin cytoskeleton plays a critical role in maintaining pericyte morphology, attachment to, and contraction of underlying substrata by microvascular pericytes.

Note that nocodazole, which inhibits microtubule polymerization, increased and maintained the microdomain stiffness, indirectly activating and coarsening the actin cytoskeleton (Fig. 3); blebbistatin and ML-7, which bind to myosin II, changed cell morphology dramatically (Supplementary Fig. 2). This may be attributable to the disturbed balance between the actin cytoskeleton and microtubules, a balance regulated by myosin II as reported by Even-Ram et al. [2], where one dominates over the other when either is inhibited.

Many researchers have suggested that pericytes play critical roles in (anti)angiogenesis [6, 7, 11, 12]. Specifically, most research results have been focused on the communication between pericytes and endothelial cells via biochemical factors such as ligand-receptor interactions. However, the present results suggest that pericytes can also directly exert

mechanical stress on adjacent endothelial cells and ECM, and may also alter the effective elastic properties of an underlying substratum via actin-mediated contraction (Fig. 5). Reinhart-King et al. [44] recently reported that endothelial cells can detect and respond to mechanical stimuli created by neighboring cells. Our observations, together with Reinhart-King et al.'s and Kutcher et al.'s results for endothelial cells [7, 44] suggest the mechanical and chemical coupling between pericytes and endothelial cells, as we outline below and show schematically in Fig. 5.

As Thompson et al. [33] have reported, mechanical properties of underlying substrata impact the adhesion of vascular endothelial cells. Others [45] have also observed changes in morphology of endothelial cells under different mechanical stimuli, potentially affecting angiogenesis.

It is thus now appreciated that the morphology, adhesion, and certain functions of vascular endothelial cells can be altered by the mechanical stiffness of extracellular materials [33, 44, 45]. A comparison can be made between ECM properties and characteristics and the stiffness and thickness of the PDMS substrata used in these studies. We consider again the basement membrane (BM), the extracellular matrix to which pericytes adhere, for which the reported uniaxial tensile stress-strain response [46] is shown in Fig. 5A. The slope of the entirety of this curve, approximating the BM's stiffness, is on the order of  $E$  of PDMS; additionally, the approximate thickness of the basement membrane is  $1\ \mu\text{m}$ , the same thickness as the PDMS used in these studies. We can therefore posit that pericytes that are adhered equally well to basement membrane have the potential to exert similar deformation as that reported here, thus supporting the concept of direct transmission of mechanical strain between pericytes and adjacent or underlying vascular endothelial cells. Furthermore, we note that the basement membrane stress-strain response is non-linear elastic, meaning that the effective stiffness ( $d\sigma/d\varepsilon$ ) is not independent of strain but is in fact a direct, and in this case, increasing function of applied axial strain. Thus it is reasonable to expect that pericyte contraction could locally deform the surrounding BM to strain magnitudes sufficient to change the effective stiffness of the basement membrane. We suggest that the pericytes' potential modification of an underlying substratum's elastic properties can influence morphological changes of endothelial cells and thus the process of angiogenesis. This pericyte-induced stiffening of the BM would expose adjacent endothelial cells to a modified mechanical microenvironment, or niche (see Fig. 5B, schematized based on Ref. [7, 26, 46]).

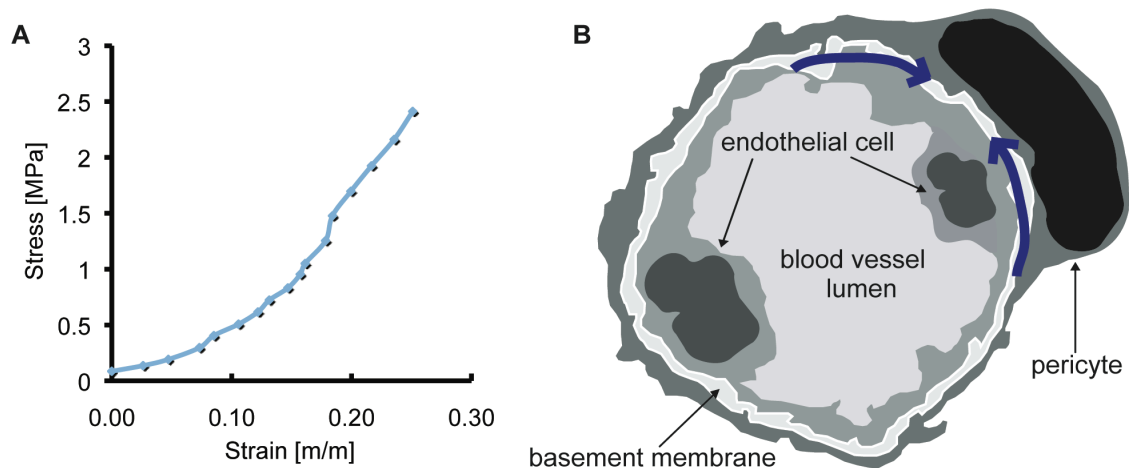


FIGURE 5 (A) The non-linear tensile stress-strain response of the basement membrane (BM), a substratum shared with vascular endothelial cells (ECs), adapted from Welling et al. [46]. Pericyte-generated strains may be sufficient to modify the effective elastic moduli of BM, which in turn would affect the microenvironment of endothelial cells. (B) Schematic of pericyte force exertion against the BM. Pericytes generate contractile force (blue arrows) that can be transmitted through the BM to adjacent ECs. Pericyte-generated strains may be sufficient to modify the effective elastic moduli of this BM, which in turn affects the mechanical microenvironment of endothelial cells.

Others have recently reported that endothelium and capillary blood vessels that are not surrounded by pericytes or smooth muscle cells exhibit an increased degree of neovascularization and angiogenesis [6, 11]. As has been observed for several adherent tissue cell types, vascular endothelial cell adhesion efficiency is modulated by the stiffness of the substratum [33]. Therefore, pericytes may alter the adhesion of endothelial cells to the basement membrane or underlying substrata, and thus inhibit neovascularization and angiogenesis that accompany morphological changes of endothelial cells on substrata. In this respect, we posit that pericyte-endothelial cell interactions relevant to angiogenesis and neovascularization would be affected not only by biochemical factors such as ligand-receptor kinetics, but also through the pericytes' exertion of mechanical forces that are communicated to nearby endothelial cells either through direct strain or indirect mechanical stiffening of the underlying nonlinear elastic substrata.

#### ACKNOWLEDGEMENTS

We gratefully acknowledge partial funding from the US National Science Foundation CAREER Award, CBET-0644846 (KJV), NIH EY 19533 (IMH) and NIH EY 15125 (IMH). We appreciate insightful discussion of buckling with Adam J. Nolte.

## REFERENCES

1. Ayscough, K.R., Stryker, J., Pokala, N., Sanders, M., Crews, P., and Drubin, D. G., *High Rates of Actin Filament Turnover in Budding Yeast and Roles for Actin in Establishment and Maintenance of Cell Polarity Revealed Using the Actin Inhibitor Latrunculin-A*. *Journal of Cell Biology*, 1997. **137**: p. 399-416.
2. Even-Ram, S., Doyle, A.D., Conti, M.A., Matsumoto, K., Adelstein, R.S., and Yamada, K.M., *Myosin IIA regulates cell motility and actomyosin-microtubule crosstalk*. *Nature Cell Biology*, 2007. **9**: p. 299-309.
3. Bergers, G., and Song, S., *The role of pericytes in blood-vessel formation and maintenance*. *Neuro-Oncology*, 2005. **7**: p. 452-464.
4. Rosenthala, R., Choritzb, L., Schlottb, S., Bechrakisa, N. E., Jaroszewskic, J., Wiederholtb, M., and Thieme, H., *Effects of ML-7 and Y-27632 on carbachol- and endothelin-1-induced contraction of bovine trabecular meshwork*. *Experimental Eye Research*, 2005. **80**: p. 837-845
5. Saitoh, M., Ishikawa, T., Matsushima, S., Naka, M., and Hidaka, H., *Selective inhibition of catalytic activity of smooth muscle myosin light chain kinase*. *Journal of Biological Chemistry*, 1987. **262**: p. 7796-7801.
6. Adams, R.H., and Alitalo, K., *Molecular regulation of angiogenesis and lymphangiogenesis*. *Nature Review Molecular Cell Biology*, 2007. **8**: p. 464-478.
7. Kutcher, M.E., Kolyada, A. Y., Surks, H. K., and Herman, I. M., *Pericyte Rho GTPase Mediates Both Pericyte Contractile Phenotype and Capillary Endothelial Growth State*. *The American Journal of Pathology*, 2007. **171**: p. 693-701.
8. Vasquez, R.J., Howell, B., Yvon, A. M., Wadsworth, P., and Cassimeris, L., *Nanomolar concentrations of nocodazole alter microtubule dynamic instability in vivo and in vitro*. *Molecular Biology of the Cell*, 1997. **8**: p. 973-985.
9. Bubb, M.R., Spector, I., Beyer, B. B., and Fosen, K. M., *Effects of Jasplakinolide on the Kinetics of Actin Polymerization*. *The Journal of Biological Chemistry*, 2000. **275**: p. 5163-5170.
10. Lázaro-Diéguez, F., Aguado, C., Mato, E., Sánchez-Ruiz, Y., Esteban, I., Alberch, J., Knecht, E., and Egea, G., *Dynamics of an F-actin aggresome generated by the actin-stabilizing toxin jasplakinolide*. *Journal of Cell Science*, 2008. **121**: p. 1415-1425.
11. Armulik, A., Abramsson, A., and Betsholtz, C., *Endothelial/Pericyte Interactions*. *Circulation Research*, 2005. **97**: p. 512-523.

12. Papetti, M., and Herman, I. M., *Mechanisms of normal and tumor-derived angiogenesis*. Am J Physiol Cell Physiol, 2002. **282**: p. C947–C970.
13. Bondjers, C., Kalén, M., Hellström, M., Scheidl, S. J., Abramsson, A., Renner, O., Lindahl, P., Cho, H., Kehrl, J., Betsholtz, C., *Transcription profiling of PDGF-B deficient embryos identifies RGS5 as a novel marker for pericytes and vascular smooth muscle cells*. Am J Pathol, 2003. **162**: p. 721–729.
14. Gerhardt, H., and Betsholtz, C., *Endothelial-pericyte interactions in angiogenesis*. Cell Tissue Res, 2003. **314**: p. 15–23.
15. Davis, M.J., and Hill, M. A., *Signaling mechanisms underlying the vascular myogenic response*. Physiol Rev, 1999. **79**: p. 387–423.
16. Davis, M.J., Wu, X., Nurkiewicz, T. R., Kawasaki, J., Davis G. E., Hill, M. A., Meininger, G. A., *Integrins and mechanotransduction of the vascular myogenic response*. Am J Physiol Heart Circ Physiol, 2001. **280**: p. H1427–H1433.
17. Falcone, J.C., Davis, M. J., Meininger, G. A., *Endothelial independence of myogenic response in isolated skeletal muscle arterioles*. Am J Physiol Heart Circ Physiol, 1991. **260**: p. H130–H135.
18. Sun, Z., Martinez-Lemus, L. A., Hill, M. A., and Meininger, G. A., *Extracellular matrix-specific focal adhesions in vascular smooth muscle produce mechanically active adhesion sites*. Am J Physiol Cell Physiol, 2008. **295**: p. 268–278.
19. Garmy-Susini, B., Jin, H., Zhu, Y., Sung, R. J., Hwang, R., Varner, J., *Integrin alpha4beta1-VCAM-1-mediated adhesion between endothelial and mural cells is required for blood vessel maturation*. The Journal of clinical investigation, 2005. **115**: p. 1542–1551.
20. Graziolia, A., Alvesb, C. S., Konstantopoulosb, K., and Yang, J. T., *Defective blood vessel development and pericyte/pvSMC distribution in a4 integrin-deficient mouse embryos*. Developmental Biology, 2006. **293**: p. 165–177
21. Galbraith, C.G., Yamada, K. M., and Sheetz, M. P., *The relationship between force and focal complex development*. Journal of Cell Biology, 2002. **159**: p. 695–705.
22. Mogilner, A., and Oster, G., *Force Generation by Actin Polymerization II: The Elastic Ratchet and Tethered Filaments*. Biophysical Journal, 2003. **84**: p. 1591–1605.
23. Takagi, Y., Homsher, E. E., Goldman, Y. E., and Shuman, H., *Force Generation in Single Conventional Actomyosin Complexes under High*

- Dynamic Load*. Biophysical Journal, 2006. **90**: p. 1295–1307.
24. Zhua, J., and Carlsson, A. E., *Growth of attached actin Filaments*. Eur Phys J E, 2006. **21**: p. 209–222.
  25. Goldschmidt, M.E., McLeod, K. J., and Taylor, W. R., *Integrin-mediated mechanotransduction in vascular smooth muscle cells: frequency and force response characteristics*. Circ Res, 2001. **88**: p. 674–680.
  26. Herman, I.M., D'Amore, P. A., *Microvascular pericytes contain muscle and nonmuscle actins*. Journal of Cell Biology, 1985. **101**: p. 43–52.
  27. Harris, A.K., Wild, P., Stopak, D. , *Silicone rubber substrata: a new wrinkle in the study of cell locomotion*. Science, 1980. **208**: p. 177–179.
  28. Kelley, C., et al., *Microvascular pericyte contractility in vitro: comparison with other cells of the vascular wall*. Journal of Cell Biology, 1987. **104**: p. 483–490.
  29. Burton, K., J. Park, and D. Taylor, *Keratocytes generate traction forces in two phases*. Molecular Biology of the Cell, 1999.
  30. Aebi, U., and Pollard, T.D. , *A glow discharge unit to render electron microscope grids and other surfaces hydrophilic*. J. Electron Microscopic Technique, 1987. **7**: p. 29–33.
  31. Butt, H.J., and Jaschke, M., *Calculation of thermal noise in atomic force microscopy*. Nanotechnology, 1995. **6**: p. 1–7.
  32. Hutter, J.L., and Bechhoefer, J., *Calibration of atomic- force microscope tips*. Rev Sci Instrum, 1993. **64**: p. 1868–1873.
  33. Thompson, M.T., Berg, M. C., Tobias, I. S., Rubner, M. F., and Van Vliet, K. J., *Tuning compliance of polyelectrolyte multilayers to modulate cell adhesion*. Biomaterials, 2005. **26**: p. 6836–6845.
  34. Thompson, M.T., Berg, M. C., Tobias, I. S., Lichter, J. A., Rubner, M. F., Van Vliet, K. J., *Biochemical functionalization of polymeric cell substrata can alter mechanical compliance*. Biomacromolecules, 2006. **7**: p. 1990–1995.
  35. Cerda, E. and L. Mahadevan, *Geometry and physics of wrinkling*. Physical review letters, 2003.
  36. Chung, J., J. Youngblood, and C. Stafford, *Anisotropic wetting on tunable micro-wrinkled surfaces*. Soft Matter, 2007.
  37. Huang, R. and Z. Suo, *Very thin solid-on-liquid structures: the interplay of flexural rigidity, membrane force, and interfacial force*. Thin Solid Films, 2003. **429**(1-2): p. 273–281.
  38. Shlomovitz, R., and Gov, N. S., *Membrane Waves Driven by Actin and*

- Myosin*. Physical Review Letters, 2007. **98**: p. 168103.
39. Harris, A., P. Wild, and D. Stopak, *Silicone rubber substrata: a new wrinkle in the study of cell locomotion*. Science (New York, 1980).
  40. Burton, K. and D.L. Taylor, *Traction forces of cytokinesis measured with optically modified elastic substrata*. Nature, 1997. **385**: p. 450-454.
  41. Balaban, N.Q., et al., *Force and focal adhesion assembly: a close relationship studied using elastic micropatterned substrates*. Nature Cell Biology, 2001. **3**(5): p. 466-472.
  42. Sabass, B., M. Gardel, and C. Waterman, *High resolution traction force microscopy based on experimental and computational ...*. Biophysical Journal, 2008.
  43. Tan, J., et al., *Cells lying on a bed of microneedles: an approach to isolate mechanical force*. Proceedings of the National Academy of Sciences, 2003.
  44. Reinhart-King, C.A., Dembo, M., and Hammer, D. A., *Cell-cell mechanical communication through compliant substrates*. Biophysical Journal, 2008.
  45. Shukla, A., Dunn, A. R., Moses, M. A., and Van Vliet, K. J., *Endothelial cells as mechanical transducers: Enzymatic activity and network formation under cyclic strain*. Mechanics and Chemistry of Biosystems, 2004. **1**: p. 279-290.
  46. Welling, L., M. Zupka, and D. Welling, *Mechanical properties of basement membrane*. Physiology, 1995.

FIGURE 1 (A) Schematic of AFM-enabled imaging and indentation. Cell and wrinkle topography was obtained from contact-mode imaging. Effective elastic moduli were determined via indentation at specific subcellular regions of interest on the pericyte, using optical microscopy to position the probe both “on” or above substrata wrinkles (B) and “off” or far from wrinkles (C). Inset images in (A)-(C) are AFM deflection images, and blue asterisks (\*) indicate corresponding locations of indentation. (D) summarizes effective elastic moduli of pericyte microdomains both on ( $16.3 \pm 3.9$  kPa) and off ( $7.4 \pm 1.1$  kPa) these wrinkles (see Methods). Error bars denote standard deviation. Scale bars = 20  $\mu\text{m}$ .

FIGURE 2 Actin-dependent alterations in pericyte shape, contractile phenotype and elastic moduli of cell microdomains. In (A), (B), and (C), AFM deflection images demonstrate changes in pericyte shape. Concomitantly, cell shape and PDMS deformation, either before or 65 min after the addition of pharmacological inhibitors that specifically affect actin (de)polymerization and/or actomyosin contraction: (A), latrunculin A (1  $\mu\text{M}$ ); (B), blebbistatin (25  $\mu\text{M}$ ); (C), ML-7 (300 nM), respectively (see Table 1). (D) demonstrates the elastic moduli of pericyte membranes, as schematized in Fig. 1 (see Materials and Methods for elastic moduli measurement), before and after addition of inhibitors, at pericyte membranes on and off deformed (wrinkled) PDMS substratum domains. Table 2 summarizes elastic moduli with inhibitors. For each condition  $n > 5$  cells were considered, and 30 indentations were acquired at each point (on or off the wrinkle positions). Error bars denote standard deviation. Scale bars = 20  $\mu\text{m}$ . Asterisk (\*) indicates statistically significant difference from all other conditions shown ( $p < 0.01$ ).

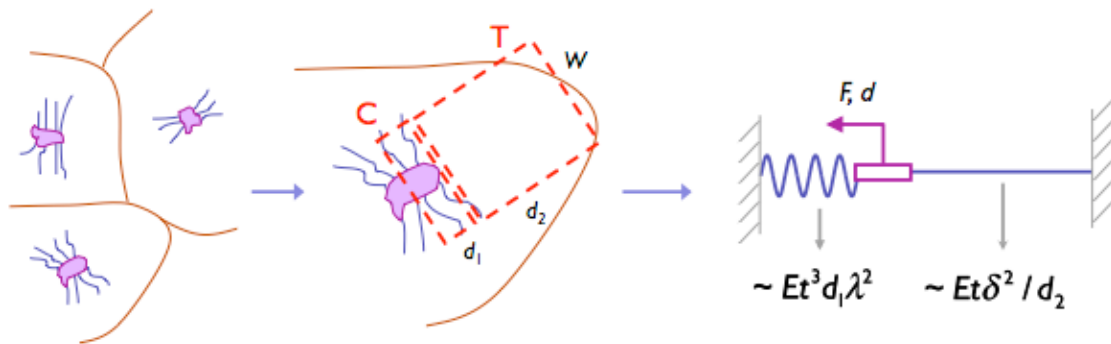
FIGURE 3 Change in elastic moduli and cell shape with addition of cytoskeleton-modulating agents. The same set of experiments as shown in Fig. 2 was conducted with pharmacological reagents that increase the activity of the actin cytoskeleton: nocodazole (670 nM) (A) and jasplakinolide (670 nM) (B): see Table 1. (C) Mechanical tests were conducted before and after addition of these reagents at cell membranes on and off PDMS wrinkles. See Table 2 for summary of elastic moduli with nocodazole and jasplakinolide. All the mechanical tests were conducted with more than five cells ( $N = 5$ ) and 30 mechanical tests ( $n = 30$ ) on and off wrinkles. Error bars denote standard deviation. Scale bars = 20  $\mu\text{m}$ .

FIGURE 4 Calculation of contraction induced by pericytes. (A) AFM contact-mode topography image indicates height changes of wrinkled PDMS substrata; inset: corresponding deflection (error-signal) image for same pericyte. Scale bar = 20  $\mu\text{m}$ . From wrinkle topography, pericyte-exerted force on the PDMS substrata can be estimated as described in the text. (B)

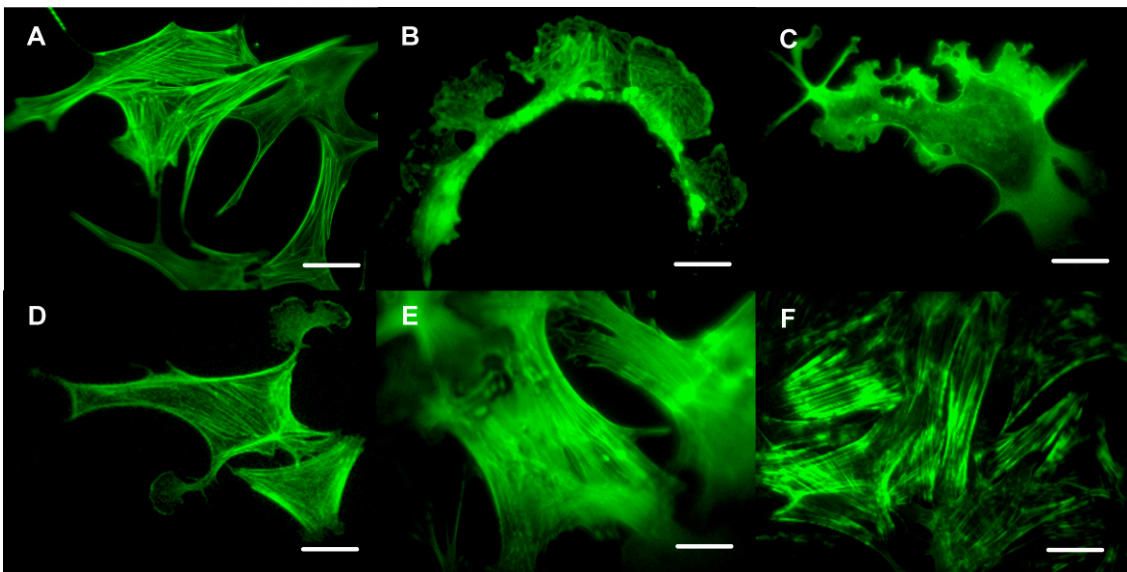


Height trace of one such wrinkle, indicated as white line in (A). Contraction of the PDMS, defined as the normalized change in length between two points due to wrinkling  $(l_0 - l_f)/l_0$ , of  $37.5 \pm 1.8\%$  was calculated from the final wrinkle span  $l_f$  and initial unwrinkled length  $l_0$  (see Materials and Methods);  $n = 71$  wrinkles. (C) Distribution of contraction observed.

FIGURE 5 (A) The non-linear stress-strain curve of the basement membrane (BM), a substratum shared with vascular endothelial cells (ECs), adapted from Welling et al. [46]. Pericyte-generated strains may be sufficient to modify the effective elastic moduli of BM, which in turn would affect the microenvironment of endothelial cells. (B) Schematic of pericyte force exertion against the BM. Pericytes generate contractile force (blue arrows) that can be transmitted through the BM to adjacent ECs. Pericyte-generated strains may be sufficient to modify the effective elastic moduli of this BM, which in turn affects the microenvironment of endothelial cells.



SUPPLEMENTARY FIGURE 1. Model of pericyte contraction on a deformable, wrinkling, substrata. Rectangular regions of contraction and tensile loading of dimensions  $d_1$  and  $d_2$  respectively are used to estimate strain energies induced by the pericyte exerted strain.



SUPPLEMENTARY FIGURE 2 Fluorescent images of F-actin-stained pericytes upon treatment with various agonists and antagonists of actomyosin-mediated cell contraction. Fixed pericytes were stained with Alexa 488 phalloidin at 37°C: (A), untreated pericytes; (B), those treated with latrunculin A (1  $\mu$ M); (C), blebbistatin (25  $\mu$ M); (D), ML-7 (300 nM); (E), nocodazole (670 nM); and (F), jasplakinolide (670 nM). Scale bars = 20  $\mu$ m.